Understanding Fluid Flow in a Microfluidic Cell Sorter using Computational Fluid Dynamics

A Thesis Submitted to the Department of Mechanical and Aeronautical Engineering at The Ohio State University as part of the Requirements for Graduation with Honors Research Distinction

Jonathan Michael Winkler

May, 2019

Abstract

Cell sorters have been a key tool in several ground-breaking medical discoveries. Their ability to sort based on different parameters simultaneously has made them valuable tools used to study the Immune System, cancers, and other complex biology. The development of a sorter introduces several questions about how accurately the device can sort cells. In this thesis, we present computational fluid dynamics (CFD) studies to analyze pressure distributions and flow rates in a new microfluidic cell sorter. The cell sorter has an actuator that changes the widths of two channels after a Y-shaped bifurcation. The actuator is controlled using an electric potential which causes an electrostatic force. To control the electric potential, De-Ionized (DI) water must be used; to maintain cells' viability, cell solution is required. These fluids must be kept in their specific channels for the sorter to operate. The small scale of the microfluidic cell sorter makes it impossible to experimentally determine pressure and velocity at several key locations in the sorter without extensive modifications to its typical operation. However, the use of CFD allows analysis of the entire fluid domain. Further, the cost and time required to make prototypes makes computational methods a desirable alternative. To understand the fluid domain in the microfluidic cell sorter, we studied two main questions: how the DI water mixes with the cell solution, and how the sorting action impacts the pressure gradients and streamlines of the fluid. Examining the Pressure gradients and streamlines of two fluids in the sorter revealed that the fluids interaction would prevent the sorter from operating without reducing the survivability of cells in the sorter.

Acknowledgements

First, I'd like to thank Dr. David Hoelzle. His passion, attention to detail, and willingness to help have shown me what it means to be a great professor and researcher. His ability to motivate without discouraging has been essential through during this project, and I can't thank him enough for the opportunity I've had to learn and work on research like this as an Undergraduate.

Next, I'd like to thank Melinda Lake. Through long meetings in the basement to last minute emails and deadlines, the help she's given me during this project has been absolutely essential. Her willingness to sit down and teach me even fundamental concepts in the middle of the day always left me feeling more confident with the problems ahead. Her patience with my often unpreparedness and helping me through deadlines cannot be appreciated enough, and there's nothing I can do to sufficiently show my gratitude.

I also would like to thank Dr. Datta Gaitonde, for introducing me to and continuing to pique my interest in Computational Fluid Dynamics since my first class with him. Coming up to your office to ask about convergence issues was always a treat, and thanks for having an open door about research, classes, BSLI, jobs, or anything else.

Finally, I'd like to thank Cynthia Dove. Through sleepless nights or early morning panicked texts she always helped me get through the most stressful times of my life. Whether it was dragging me out of the house to get some dinner, or just letting me work while we watched TV, her understanding, caring, and compassion always made my life's stressful moments not just bearable but enjoyable.

Contents

List of Figures

List of Tables

1 Introduction

For any new cell sorting device to become an accepted tool by researchers, it must be proven to sort cells reliably at its maximum sorting frequency. During the design phase of a project, the maximum frequency of the sorter design will be estimated and the fluid's behavior during the sorter operations will be better understood. To be considered successful, the project should either indicate that the sorter can operate at a given frequency or give reasons why the sorter would not work. It is hoped that the findings of our research will inform of potential changes that can be made to improve the performance of the sorter. As such, we introduce some applications of cell sorters in Section 1.1 as well as examples of existing cell sorters in Section 1.2. In Section 1.3 we discuss the relevance of Computational Fluid Dynamics (CFD) as a tool to test cell sorting designs.

1.1 Uses of Cell Sorters

Cell sorters have advanced modern medicine in several ways. They are primarily used as a tool to form populations of cells based on measured phenotypes for follow-up assays. For example, researchers used cell sorters to better understand the interplay between T and B cells. Lymphocytes were known to exist but the way they operated was not fully understood until cell sorting allowed T and B cells to be sorted[1], [2]. This primitive method of cell sorting selectively adhered cells based on their phenotypes to a petri dish. The cells could then be pipetted individually after adhesion occurred. Sorting lymphocytes since then has become faster and more efficient using a Magnetic Activated Cell Sorter (MACS) [3]. The ability to examine the immune system played a vital role into AIDS/HIV research and diagnosis [4]. Cell sorting allowed clinicians and researchers to categorize the diseases effect on the immune

system, specifically the effect of HIV CD4+ T lymphocytes in the peripheral blood. If the CD4+/CD8+ T count falls below a certain point, it is a good indicator of infection and stage of infection. [5]

1.2 Cell Sorting Methods

One of the industry standards for sorting large populations of cells is the Florescence Activated Cell Sorter (FACS), which will detect and sort cells based on their measured florescence. FACS typically detects and sorts at approximately 10^4 cells/second and can be automated to allow ease of use [6]. The operating mechanism of FACS is dielectrophoresis (D) , during which cells are captured by an ionized fluid in individual droplets which move through an immiscible working fluid [7] (Figure 1). The droplets containing the cells move past electrodes that are supplied with an electrical charge when a desired phenotype is detected which biases the path of the cells into one of two channels based on its phenotype [6].

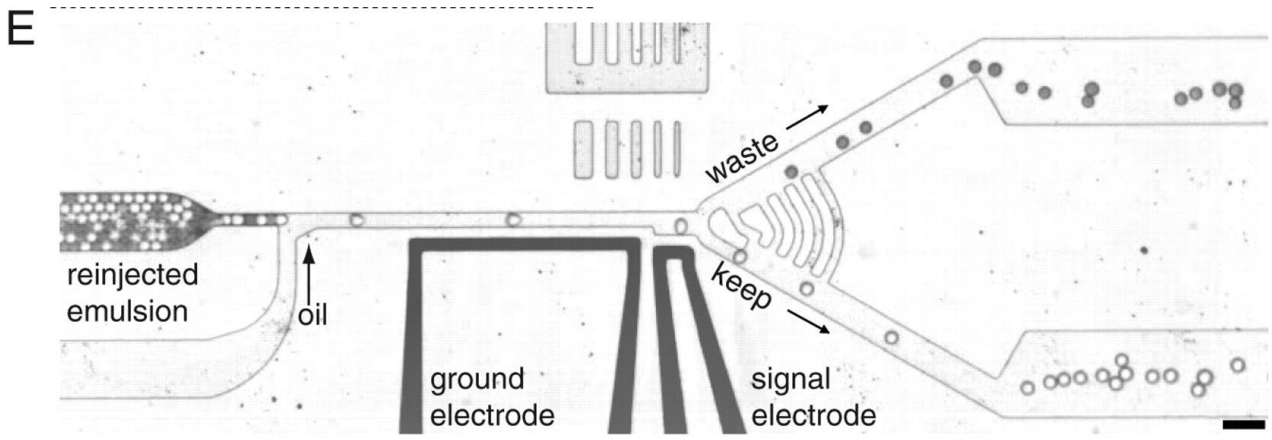

Figure 1,Example of dielectrophoresis operating mechanism shown in a fluorescence-activated microfluidic cell sorter.

When a cell is detected as waste, the cells move into the upper channel because the hydrodynamic resistance of the upper channel is lower. When a cell is detected to keep, the signal electrode activates excreting a body force on the fluid encapsulating the cell pulling into the lower channel. FACS Device as Lab-on-chip [6]

While FACS operate with a fast sorting frequency, the cells must be encapsulated in an ionized fluid and must be treated to allow fluorescence for a given phenotype. Lab-on-chip cell sorters utilize micron scale channels that are filled with a working fluid. The working fluid transports cells through the sorter and both the fluid and the cells in the fluid can be controlled. Using valves allows the sorter to control the hydrodynamic resistance in the channels which can be used to bias the path a cell will take. Other sorting methods have been developed and are plotted in Figure 2 with their typical operational Sorting Frequency.

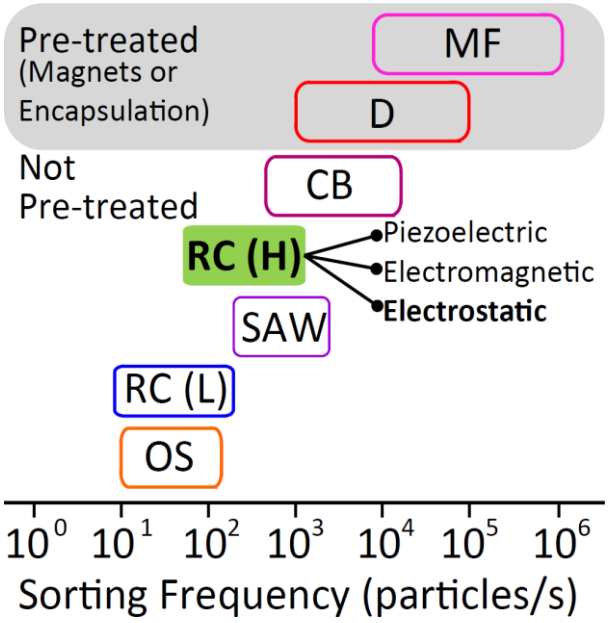

Figure 2, Methods of Sorting Cells and Their Typical Sorting Frequencies.

In order from top to bottom, they are Magnetic Fields (MF) [8], Dielectrophoresis(D)[6], Cavitation Bubbles (CB) [9], High Bandwidth Resistance Change (RC(H)), Surface Acoustic Waves (SAW) [10], Low Bandwidth Resistance Change (RC(L))[11], and Optical Switches (OS) [12].

A Mechanically Activated Phenotyping and Sorting (MAPS) device to sort cells based on their mechanical properties such as Young's Modulus is being developed. Although the focus of this thesis is the analysis of the sorting mechanism, the detection method and frequency are important to the overall effectiveness of the MAPS device. To support a high throughput of cells

at around 1000 cells/second, the High bandwidth resistance change sorting method was chosen. Specifically, the electrostatic sorting method was chosen because both the sorter and detector are electronically driven. Having both systems electrically controlled simplifies integration of the sorting device with the phenotyping mechanism onto a single lab-on-a-chip device.

1.3 Use of Computational Fluid Dynamics in Microfluidics

Understanding the fluid dynamics inside of the cell sorter is important for understanding how the actuator motion will affect the sorting outcome at the bifurcation. Obtaining consistent and reliable velocity and pressure measurements inside of the cell channels with standard methods such as pitot probes is infeasible. Methods such as Laser Doppler Velocimeters [13] are more expensive and don't allow measurement at all locations, so a computational method is preferred. Computational Fluid Dynamics (CFD) packages such as ANSYS Fluent offer a solution that calculates primitive variables at all locations in the fluid domain without interfering with the flow like many experimental methods such as pressure probes. In conjunction with qualitative experimental results, CFD offers a method of analysis to rapidly test new design ideas and obtain otherwise unobtainable results. Pressure, velocity, and other primitive flow variables can be analyzed at key points to predict how consistently the sorter will operate with given parameters.

2 Sorter Design

2.1 Resistance Change Principles

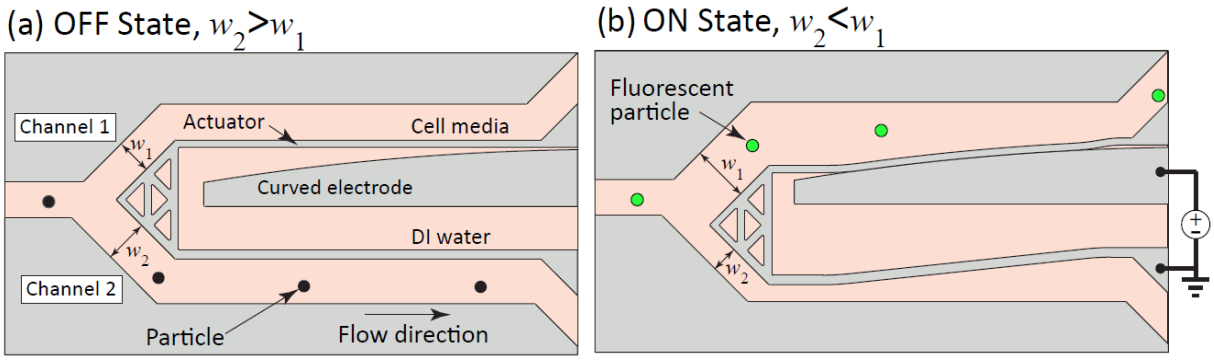

Figure 3, Schematic of MEMS Cell Sorter.

The left panel describes the sorter in the OFF state with no voltage potential applied. The right describes the sorter in the ON state with a voltage potential applied. To maintain the electrostatic force, DI water is injected into the DI water channel that is between the curved electrode and the actuator. The cell media occupies channels 1 and 2 to maintain cell viability. Image provided courtesy of Melinda Lake et al.

Cells suspended in a cell medium move down a main channel towards a bifurcation in the design shown in Figure 3. The cell sorter provides control over the cells by altering the width of two channels past the bifurcated single channel. In the "OFF" State, channel 2 is wider than channel 1 which biases the fluid and cells to move downward into channel 2. In the "ON" State, the actuator moves down increasing the width of the channel 1 while decreasing the width of the channel 2. The motion of the actuator is triggered by applying a voltage difference between the curved electrode and actuator seen in Figure 3. When the voltage difference is applied, the actuator beam is attracted to the curved electrode, moving to the ON state. Both changes in the channel widths alter the bias of the cells' path to channel 1. The relationship between channel width and fluid flow are defined by the principles of hydrodynamic resistance. When the channel width, w, is less than the channel height, h, ranging from $0 \leq w/h \leq 1$, the

Equations 1 and 2 approximate the Volumetric Flow Rate, Q, in rectangular channels as the pressure flowrate relationship.

$$Q = \frac{hw^3\Delta p}{12\mu L}\left[1 - 6\left(\frac{w}{h}\right)\sum_{n=0}^{\infty}\lambda_n^{-5}\tanh\left(\frac{\lambda_n h}{w}\right)\right] \quad \textit{Equation 1}$$

$$\lambda_n = \frac{(2n+1)\pi}{2} \quad \textit{Equation 2}$$

where L is the Channel Length, μ is the Fluid Dynamic Viscosity, and Δp is the Channel Pressure Drop [14].

The dependence of the Volumetric Flow Rate on width is approximately cubic, meaning that the width strongly effects the hydrodynamic resistance in that channel and therefore the Volumetric Flow Rate. Further, it is easy to modify the channel width from a manufacturing standpoint.

2.2 Operation

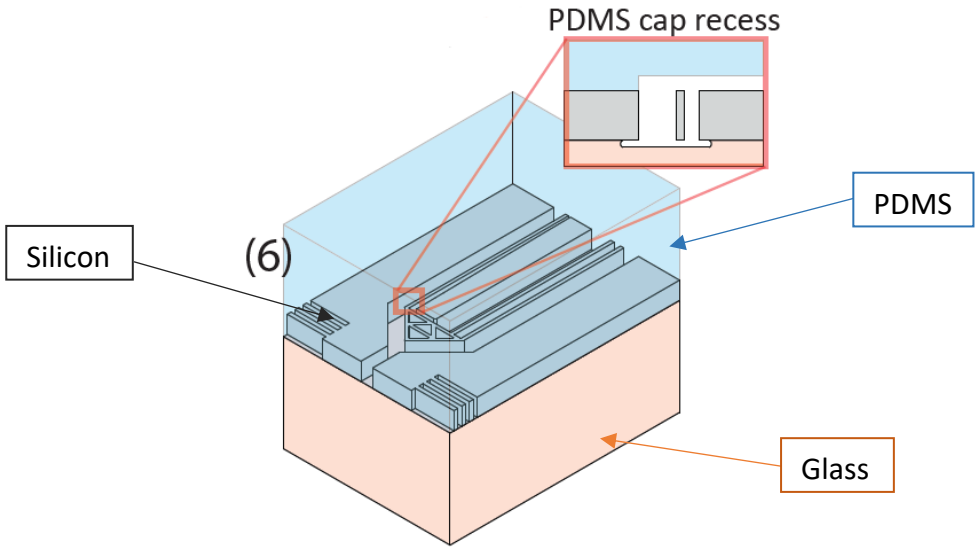

Figure 4, Schematic of fabricated sorter.

The inset shows gaps above and below actuator formed during the fabrication process. The lower gap comes from hydrofluoric acid selectively wet etching glass. The top gap is formed by bonding a PDMS cap with a recess over the actuator region.

To operate, the actuator must be allowed to move inside the cell sorter. To allow movement, a gap is formed above and below the actuator (Figure 4) [15]. During the cell sorter's operation, both DI water and Cell Solution must be in contact with each other while remaining in their specific channels (Figure 4 and Figure 3). Should too much DI water spill into the Cell channels, the cells could die which would reduce the number and variety of follow up assays available after sorting. However, if too much Cell Solution spills into the DI water channel the Ionic solution will prevent actuator motion [16]. Controlling the two fluids is difficult even in static operations because the flows are impinging and can interact at the interface above and below the actuator. During dynamic operation, mixing is worsened by the lateral movement of the actuator in the flow. To control the fluids, the flow rates of the DI water channel and the cell channel are controlled independently from each other. For the sorter to run properly, the

correct ratio between the flow rates of both channels must be determined. This thesis presents a study of the flow mixing for one design iteration of the cell sorter device.

Another important operational constraint is the fluid's reaction to the sorter's movement. As the sorter moves in the working fluid, large pressure gradients can become present which can cause misaligned streamlines, stagnation points in the sorting channels, or even reversed flow in the channels after the bifurcation. The fluid's reaction to the sorter's actuation will be a limiting factor to the speed at which the sorter can operate.

3 Methods

To analyze how the sorter operates, the analysis is split into two smaller problems: How do the fluids in the sorter mix with each other, and how does the fluid in the sorter react to the motion of the sorter. Section 3.1 reviews preliminary experimentation that was used as reference for the CFD analysis conducted in this thesis. Section 3.2 lays out basic assumptions for both models. Section 3.3 discusses the specific set up used to determine how the fluids in the sorter interact. Section 3.4 discusses the set up for the fluid's reaction to the actuation of the sorter.

3.1 Reference Experimentation

Melinda Lake manufactured and tested a preliminary cell sorter design to investigate DI water and cell solution mixing around the actuator. The gap above the actuator was not created for this test, however the gap underneath the actuator remained present. Two syringe pumps (Pump 11 Elite, Harvard Apparatus, Holliston, MA, USA) regulated the flow rates into the DI water and cell media inlets, pumping fluid from syringes connected to PEEK tubing (Idex

Health & Science, Oak Harbor, WA, USA) (Figure 5). The channels were observed on an inverted microscope (Axio A1 Observer, Carl Zeiss Microscopy, Jena, Germany) with a high-speed camera (Miro M110,Vision Research, Wayne, NJ, USA). Testing solutions were clear DI water and Blue food dye, both mixed with a surfactant, 0.01% v/v Pluronic F-127. Devices were primed using the following method where at each step, one or both syringes were replaced at each step as indicated: (1) methanol was flowed into both inlets until air bubbles were removed, (2) DI water and surfactant was flowed into both inlets until the air bubbles were removed, and (3) Blue food coloring was flowed from the second inlet (corresponding to the cell media inlet). Dowel rods were inserted into the outlet channels in place of outlet tubing and were used to facilitate air bubble removal when needed. Once the food coloring was loaded, we set both syringe pumps to 1 $\frac{mL}{hr}$ for 3 minutes before stepping down to a flow rate ratio of 25:50 $\frac{\mu L}{hr}$ (cell media/blue:DI water/clear fluid inlets). Images were captured throughout the experiment, stepping to the flow rate ratios from one to the next after a 10 minute time span: 25:10, 25:20, 25:25, 25:30, 25:35, 25:40, and 25:25 mL/hr. Only results from the 25:10, 25:30, and 25:40 $\frac{\mu L}{hr}$ flow rate ratio treatments are reported in this thesis as they are related to the CFD analysis.

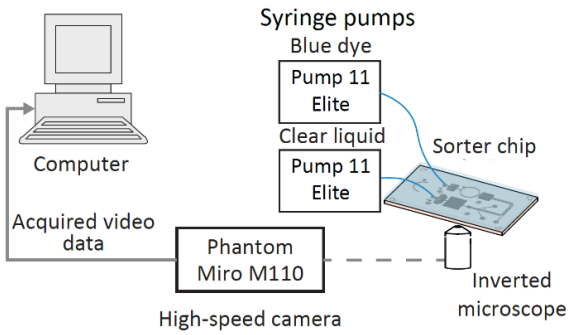

Figure 5,Experimental Setup Schematic.

Two syringe pumps flow different fluids into the sorter chip inlets. The channels are observed through an inverted microscope with an attached high-speed camera. Image provided courtesy of Melinda Lake.

3.2 Overarching Assumptions for CFD

The convergence criterion selected for these tests was 1×10^{-3} for the momentum and continuity convergence metrics, which is sufficient for Qualitative results [17]. Because the working fluid is a liquid and because the maximum pressures experienced were on the order of hundreds of pascals, the flow was assumed to be incompressible and the energy equation was not required. Laminar flow was deemed sufficient due to the low velocities, small distance scales, and high viscosity in the channels. The Reynolds number was 1.2×10^{-5} during normal operation and 20 during sorting transients, both of which are well within the range of laminar flow. To study both steady state behavior and transient behavior, the time sensitive transient formulation of the Navier-Stokes Equations were used.

3.3 Multiphase Analysis

3.3.1 Geometry and Mesh

To simplify the sorter geometry, some detailed features have been removed or simplified in the CFD model. The structural struts inside the actuator head have been fused into a solid assembly and the lower beam springs have also been simplified into a single beam. The width of the channel 2 is 37 microns while the width of channel 1 is 30 microns. The design features simplified are highlighted in Figure 6 and the final Geometry with Inlets and outlets is shown in Figure 7.

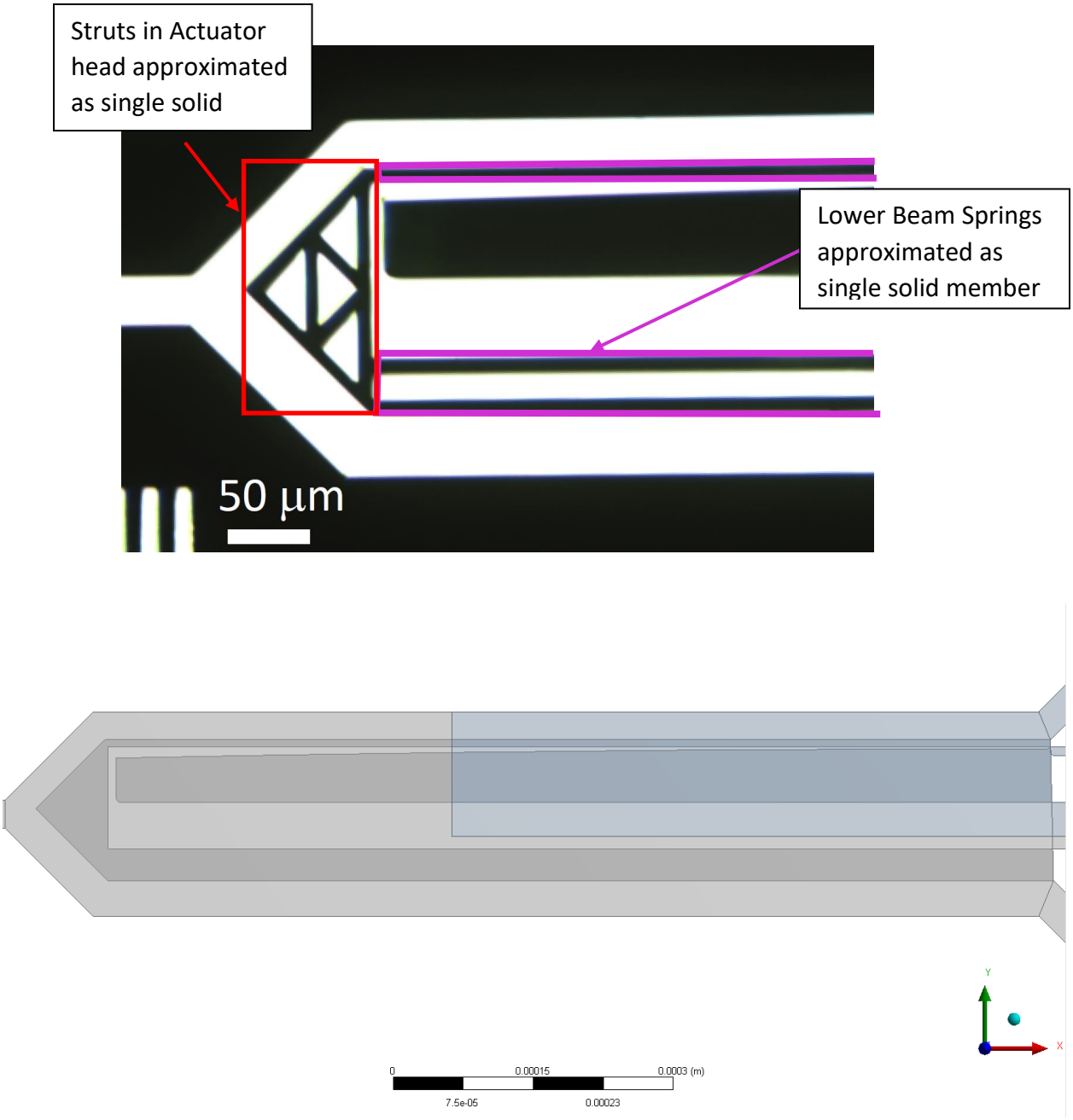

Figure 6, Microscope image of the Simplifications of Original Cell Sorter Geometry Used for Multiphase Analysis Shown compared to Microscopic Image of Cell Sorter.

modified from Image given courtesy of Melinda Lake et al.

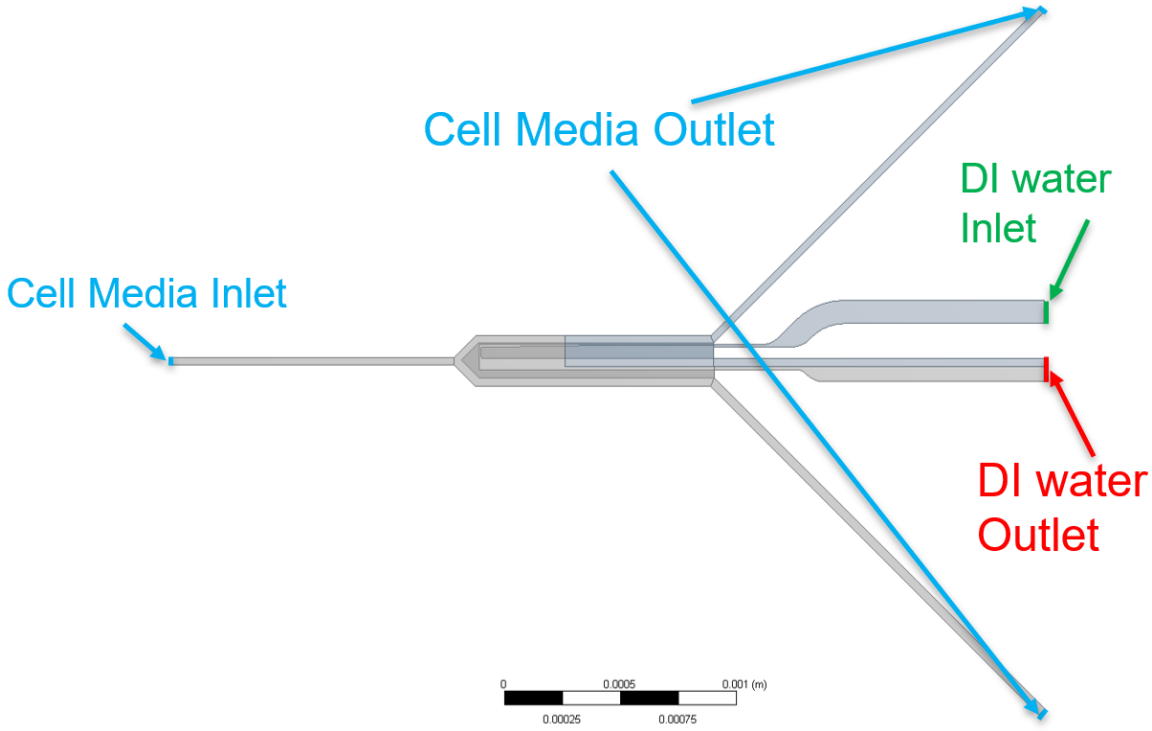

Figure 7, Geometry used in CFD for Multiphase Analysis

The mesh generated had two different inflation layers: in the channels, and above and below the actuator. A global sizing constraint of 5 microns was set to help ensure that proper mesh density was maintained across the sorter. Above and below the actuator the mesh element size was constrained to 4 microns, and an inflation layer was made with a total width of 4 microns. Along the upper DI water channel just below channel 1, the mesh was reduced to 0.8 microns with a smaller mesh of 0.5 microns at the far right where the channel is the smallest. These settings are shown in Figure 8 and Figure 9 and the corresponding numerical values used to define these mesh controls are shown in Table 1 and Table 2. These settings allowed the same number of elements to span both wide and narrow channels. The mesh generated had 1122291 nodes, and 4287349 elements. The mesh had an average orthogonal quality was 0.863, which is sufficient for typical operation [18].

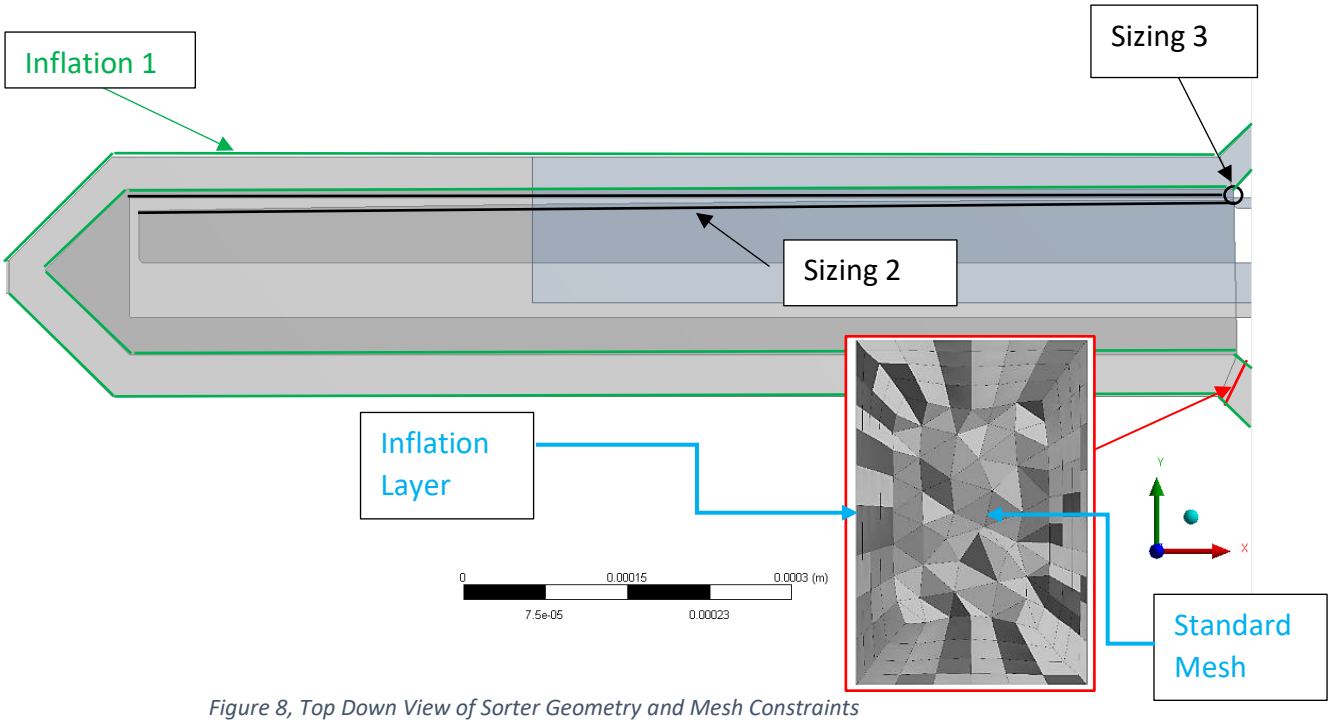

Figure 8, Top Down View of Sorter Geometry and Mesh Constraints

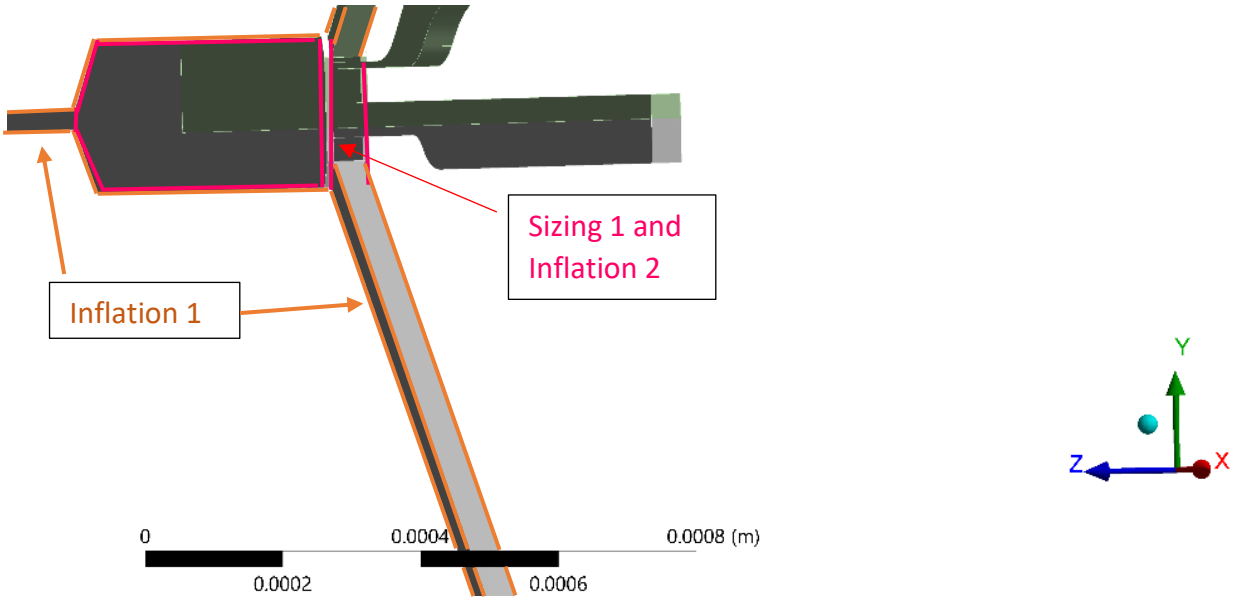

Figure 9, Side View of Sorter Geometry and Mesh Constraints

Table 1, Meshing Size Constraints used in Multiphase Analysis

Mesh Control Type	Element Sizing (m)	Inflation rate (non-dimensional)
Sizing 1	4e-6	1.2
Sizing 2	8e-7	1.2
Sizing 3	5e-7	1.2
Global	5e-6	1.2

Table 2, Meshing Inflation Layer Constraints used in Multiphase Analysis

Mesh Control Type	Total Inflation Layer Height (m)	Elements per Layer	Inflation rate (non-dimensional)
Inflation 1	10e-6	4	1.3
Inflation 2	4e-6	4	1.2

3.3.2 Solver Settings

To determine the optimal flow ratio of the Cell Solution to DI water based on CFD analysis, three sets of flow rates were tested: 25: 10, 25: 30, and 25: 40 $\frac{\mu L}{hr}$. The simulations with these flow rate ratios ran as a transient simulation for 264 seconds of flow time to reach steady state. The Volume of Fluid (VOF) model was used to simulate two distinct phases set with the physical properties of water: DI water and Cell Solution. VOF treats the fluids as immiscible, and only requires the momentum equation to be calculated for each distinct phase [19]. The VOF model was chosen over the other more advanced models available in Fluent because of the expected timescales for mixing. The DI water and cell media are expected to interact with each other on the order of a tenth of a second before moving downstream.

For the same Flow rate ratios, two different steady state conditions were reached in experiments. While some error is expected in experimentation, the large difference of steady state behavior was deemed worth investigating. One result had a stagnation point further

downstream of the bifurcation, while the other distribution stagnated near the bifurcation and this behavior was observed during a variety of tests. The 25:25 $\frac{\mu L}{hr}$ Experimental results that show two different distributions are shown in Figure 10.

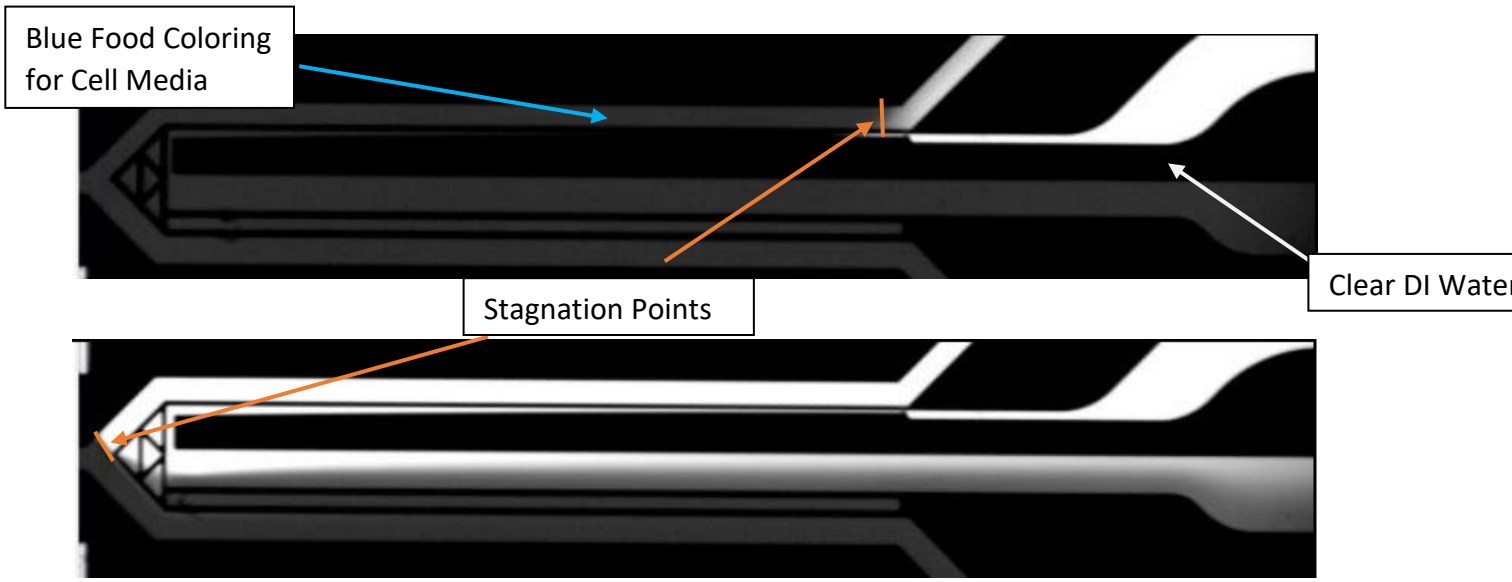

Figure 10, Different Experimental Fluid Distributions for 25:25 Cell Media:DI water flow Ratios

To attempt tripping the flow into the further forward steady state distribution, the second initial distribution was defined with DI water further forward in the cell media channel. The two different initial distributions were tested and run for 50 seconds. While 50 seconds was not enough time for the entire fluid domain to reach steady state the region of interest around the stagnation point remained steady after 50 seconds.

3.4 2D Transient Analysis of Flow around actuator

To determine how quickly the fluid in the sorter can respond to the actuation, a transient model of the actuator in motion in the fluid domain was developed. This will be helpful in determining the maximum sorting frequency possible for the cell sorter based on limitations of working in an aqueous environment.

3.4.1 Geometry and Mesh

The geometry of the sorter was further simplified in the dynamic analysis. The Geometry was defined in only two dimensions to simplify the problem. Also, to focus on the actuator's influence on the fluid domain, the DI water channel was removed since in 2D flow there is no gap to allow mixing. The width of the channel 2 is 37 microns while the width of channel 1 is 30 microns. The design features simplified are highlighted in Figure 11 and the final Geometry with Inlets and outlets is shown in Figure 12.

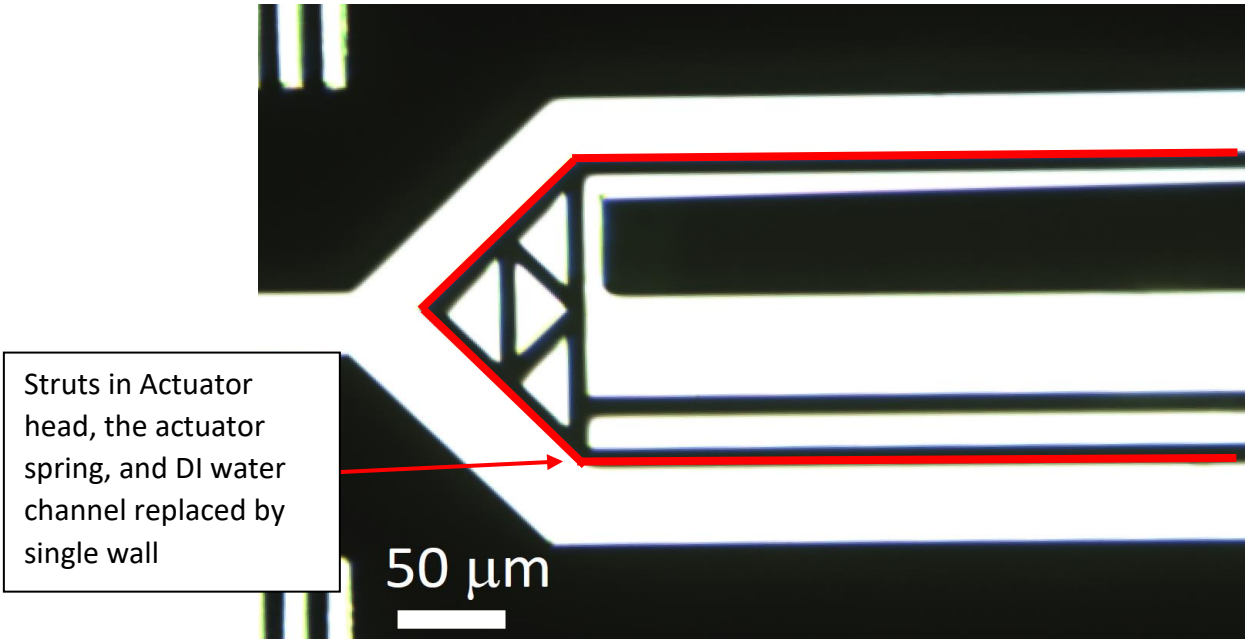

Figure 11,Simplifications of Original Cell Sorter Geometry Used for Transient Analysis Shown on Microscopic Image of Cell Sorter. Image provided courtesy of Melinda Lake et al.

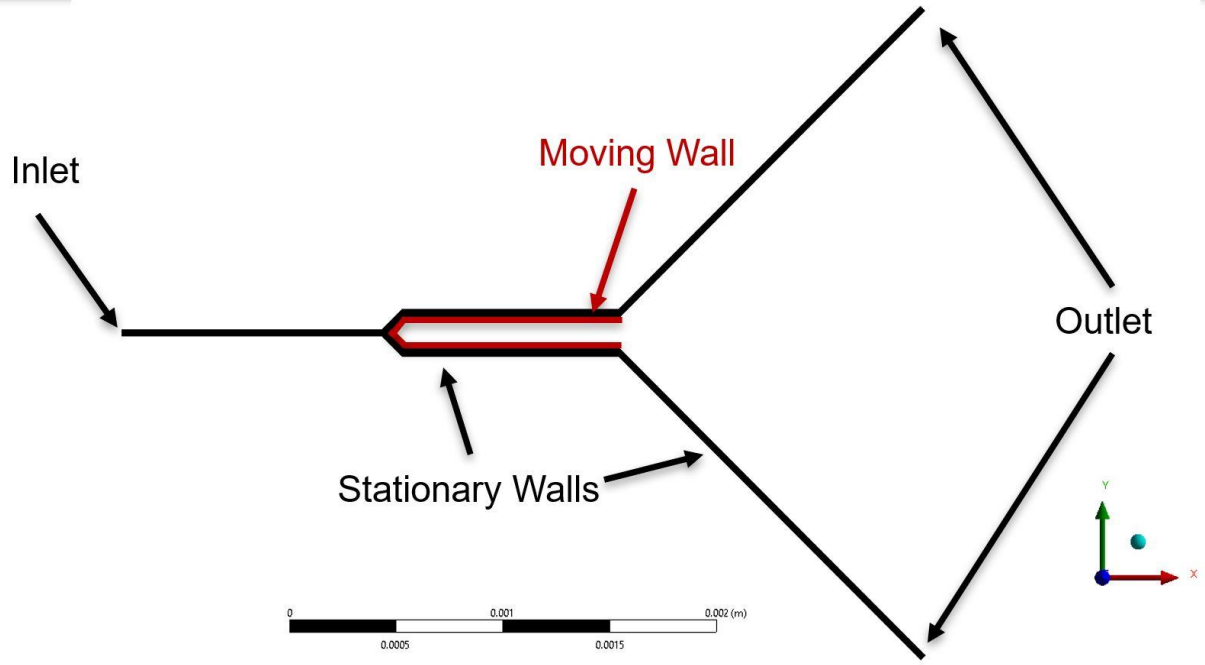

Figure 12, Geometry used in CFD for Transient Analysis

To model the sorter in motion the dynamic meshing method was utilized with Smoothing and Remeshing dynamic meshing methods. The Smoothing dynamic mesh methods are based on compressing or stretching mesh elements in the direction of the mesh motion, like springs. Smoothing dynamic meshing allows the entire mesh to change and adapt to moving boundary conditions but requires triangular elements to be used. Remeshing regenerates the mesh when minimum or maximum sizing limits are reached or when the mesh quality metrics reach a prescribed minimum. The smoothing method was called by the dynamic mesher until elements became either too small or too degenerate, in which case the remeshing method handled the mesh.[20]

The initial mesh was made with edge sizings along all the walls of 1.5 microns and an inflation rate of 1.2 while the global inflation rate is 1.3 (Table 3). Finally, all mesh elements were set to triangular to ensure the smoothing method worked through the entire mesh (Figure

13). The mesh generated has 50345 nodes and 90669 elements. The minimal orthogonal quality was 0.56 and the average quality was 0.93.

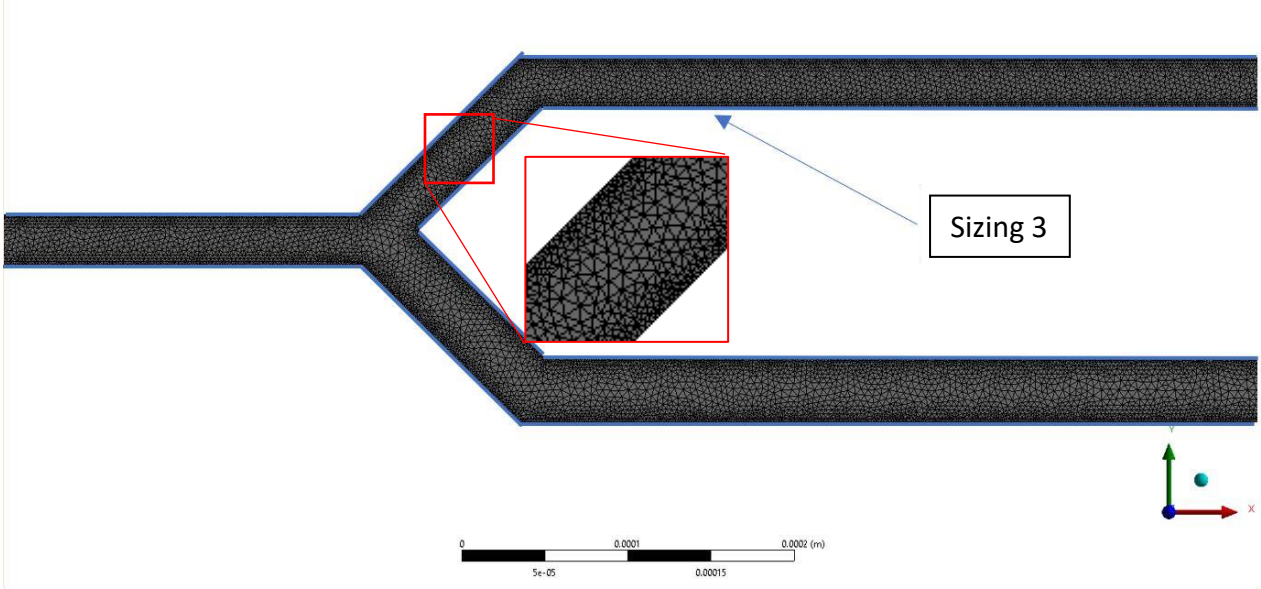

Figure 13, Initial Dynamic Mesh

Table 3, Meshing Constraints for Dynamic Mesh

Mesh Control Type	Sizing (m)	Inflation rate (non-dimensional)
Sizing 3	1.5e-6	1.2
Global	5e-5	1.3

3.4.2 Moving Wall Definition

To control the sorter motion, a User Defined Function (UDF) was developed and imported into Fluent. The UDF was called at each discrete timestep and used to calculate the required rotational velocity to control the actuator at each time step. To reduce complexity of the sorter dynamics, a few simplifying assumptions were made. First, rather than modeling the full

bending motion of the actuator beam, the actuator is modeled as a rigid body (Figure 14). To mitigate negative volume errors encountered when walls interact with each other, the center of rotation was selected as the bottom right end of the supporting beam (Figure 14).

.

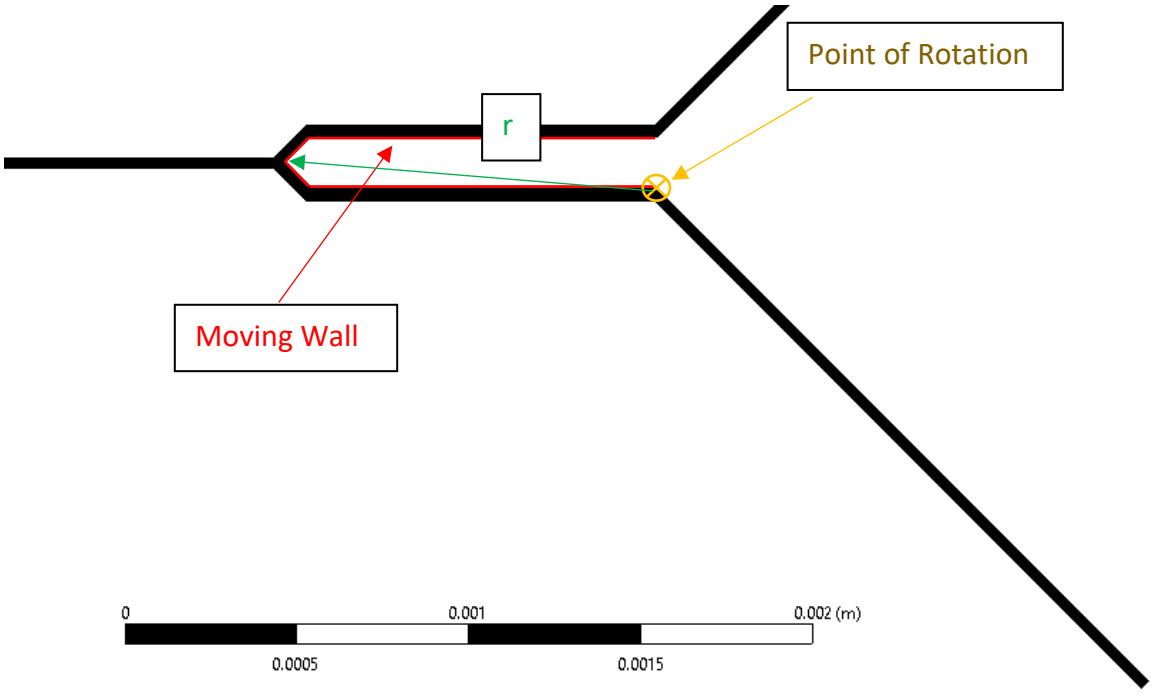

Figure 14, Dynamic Mesh Motion Set-up

Putting the center of rotation there ensured that walls would either move away from other walls or return to the "OFF" location. By defining the angular velocity as a function of time, the UDF approximates the motion of the sorter based on modeling the actuator as a mass-spring-damper system. The associated transfer function is shown in Equation 3

$$G(s) = \frac{1}{ms^2+bs+k} \qquad \textit{Equation 3}$$

where m, b, and k are defined in Table 4.

We modeled the system step response as a linear response to a high frequency square wave represented by a Fourier series approximation in Equation 4.

$$f(t) \approx \frac{1}{2}A + \sum_{i=1}^{\infty} \frac{A}{\pi k}(1 - \cos(\pi i))\ \sin(\omega t) \qquad \textit{Equation 4}$$

The corresponding actuator displacement,$X_{ss}(t)$ is represented in Equation 5. The magnitude, $|G(j\omega)|$, and phase, $\sphericalangle G(j\omega)$, are calculated using Equation 7 and Equation 8Equation 7 respectively. The Fourier Transform Frequency ω is calculated from Equation 6.

$$X_{ss}(t) = \frac{1}{2}A|G(j\omega)| + \sum_{i=1}^{\infty} \frac{A}{\pi i}(1 - \cos(\pi i))\ |G(j\omega)| \sin\left(\omega t + \sphericalangle G(j\omega)\right) \qquad \textit{Equation 5}$$

$$\omega = \frac{2\pi i}{T} \qquad \textit{Equation 6}$$

$$|G(j\omega)| = \frac{1}{\sqrt{(-m\omega^2 + k)^2 + (b\omega)^2}} \qquad \textit{Equation 7}$$

$$\sphericalangle G(j\omega) = -\tan^{-1}\left(\frac{-b\omega}{-m\omega^2 + k}\right) \qquad \textit{Equation 8}$$

The fluent UDF specified for rigid body motion only accepts velocity or angular velocity as input variables. By taking the time derivative of the position and assuming a constant lever arm, the angular velocity, $V_r(t)$ of the actuator can also be determined from Equation 9.

$$V_r(t) = \frac{1}{r}\left(\sum_{i=1}^{\infty} \frac{2A}{T}(1 - \cos(\pi i))\, |G(j\omega)| \cos\left(\omega t + \sphericalangle G(j\omega)\right)\right)$$ *Equation 9*

Table 4, values used in Equation 4-Equation 9

Variable	Definition
m	$1.6455 \times 10^{-9}\ kg$
b	$1.96233 \times 10^{-3}\ \frac{N\ sec}{m}$
k	$9.47\ \frac{N}{m}$
A	10 Volts
r (Figure 14)	0.00234 m

Because the UDF captures the approximate dynamics of the sorter, as the frequency is increased, the actuator has less time to respond to the input. At a certain frequency, the sorter is no longer able to actuate to the desired displacement because the actuator cannot move fast enough before the next actuation command is given. To compare the relative maximum displacements of the sorters, the plot of displacement and rotational velocity were plotted relative to a time normalized by the sorting period in Figure 15 and Figure 16.

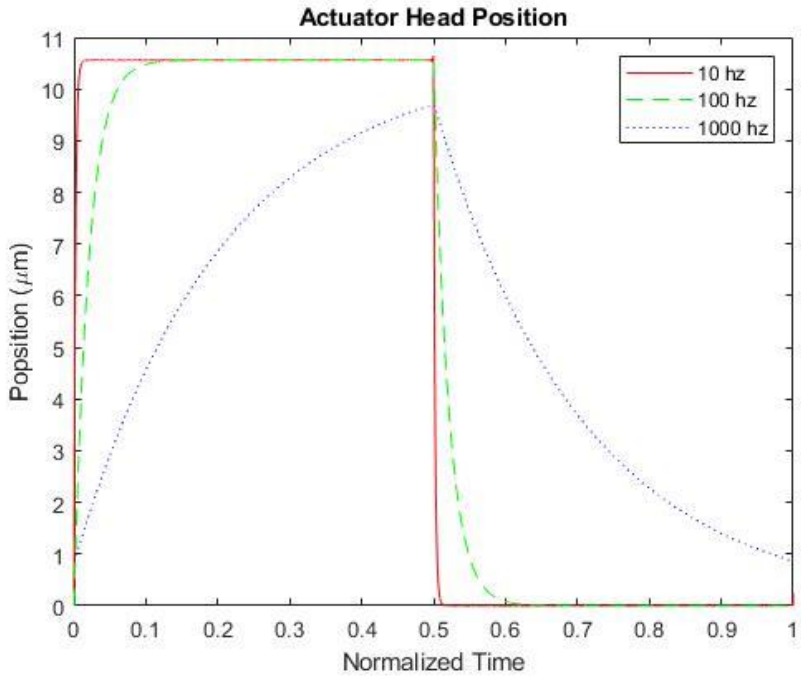

Figure 15,Actuator Position vs. Sorting Period from Equation 5

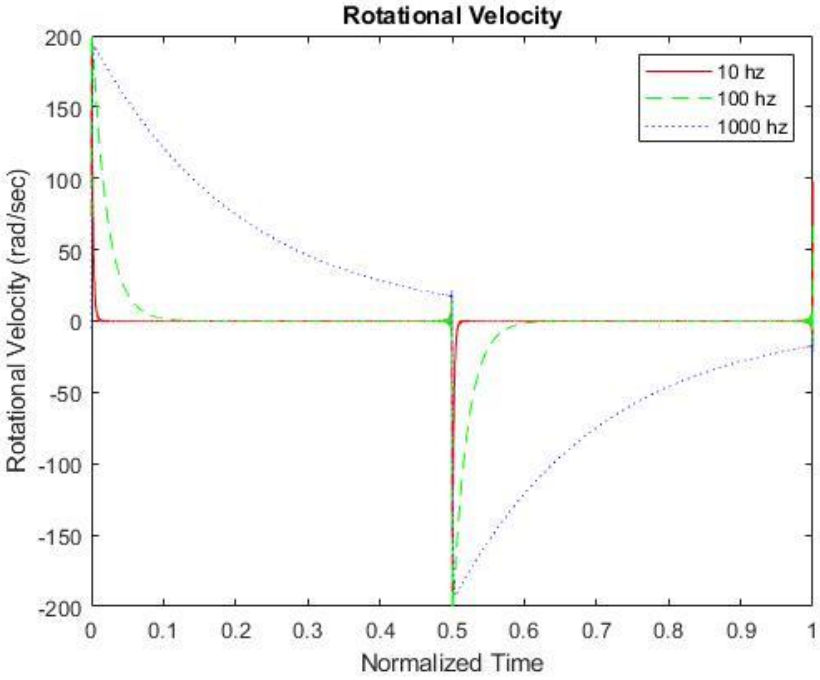

Figure 16, Actuator Rotational Velocity vs. Sorting Period from Equation 9

A threshold was necessary for the UDF because of the Gibbs phenomenon present in the Fourier series approximation of the actuator motion. Without a minimum rotational velocity, the Gibbs phenomenon caused large pressure spikes when the actuator shouldn't be moving, and the flow remained unstable and dominated by the Gibbs phenomenon. Finally, a delay was implemented to allow the flow to come to steady state before actuations begin. The effects of the threshold and delay are labeled on the raw UDF output in Figure 17.

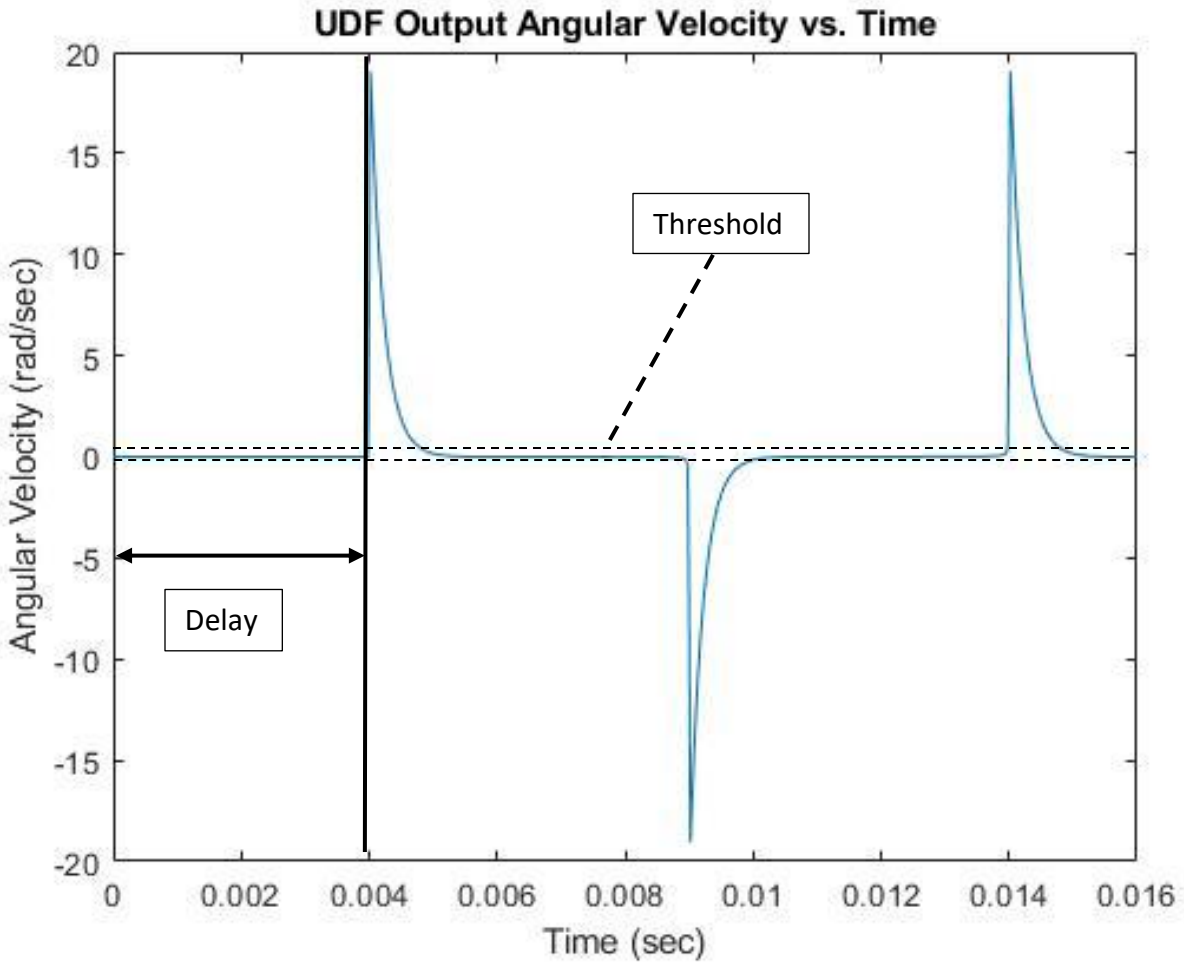

Figure 17, Angular Velocity of Actuator tip vs. time at 100hz from Equation 9 to demonstrate phases of UDF.

3.4.3 Settings

Each timestep was allowed 300 iterations to converge. The simulation was run for either two full sorting cycles or until approximately 3000 total timesteps were run. The data was saved every fifth timestep to reduce storage issues while maintaining accuracy of the solution. By saving the complete data set, post processing of the data was flexible and could be changed without the need of recalculating the solution. The two-dimensional sorter model was tested at three sorting frequencies: 10hz, 100hz, and 1000hz. The UDF allowed the flow to settle initially for 0.04 seconds before activating. The timesteps and duration of the tests were altered depending on the sorting frequency but for each test at least two full sorting cycles were simulated. These timesteps are shown in Table 5.

Table 5, Sorting Frequency and Associated Timestep

Frequency (Hz)	Timestep (s)
10	2e-5
100	1e-5
1000	5e-5

3.4.4 Sorting Metric

The primary goal of conducting transient analysis is to determine the maximum sorter frequency possible in the current design. Quantifying how quickly the sorter can operate depends on several variables. The two most important variables were assumed to be the pressure at the bifurcation of the main channel and the relative mass flowrate of the two cell channels. The average pressure was calculated in the region of interest (Figure 18). We also calculated the mass flow in Channel 1, $\dot{m}_{Ch.1}$, and Channel 2, $\dot{m}_{Ch\ 2}$, and computed a mass flow rate metric, X,

$$X = \frac{\dot{m}_{Ch.1} - \dot{m}_{Ch\,2}}{|\dot{m}_{Ch1}| + |\dot{m}_{Ch2}|}$$ *Equation 10*

to compare the mass flow rates through both channels. Equation 10 compares the mass flow through both channels of the bifurcation (Figure 18) and normalizes that flow to the total mass flow through the bifurcation. The mass flow metric is designed to capture the fluid's reaction to the actuator motion and to measure the time required for the fluid's streamlines to reestablish.

Quantifying streamlines was done by examining the mass flow through channel 1 and channel 2. Mass flow was chosen to represent the streamlines because in incompressible fluids the stream function is defined with the continuity equation [21]. The key area of interest are channels 1 and 2 just downstream of the bifurcation; the difference between these mass flow rates are related how much flow is biased in channel 1 relative to channel 2. Normalizing the difference in mass flows by the total mass flow through both channels builds in information about the origin of the streamlines.

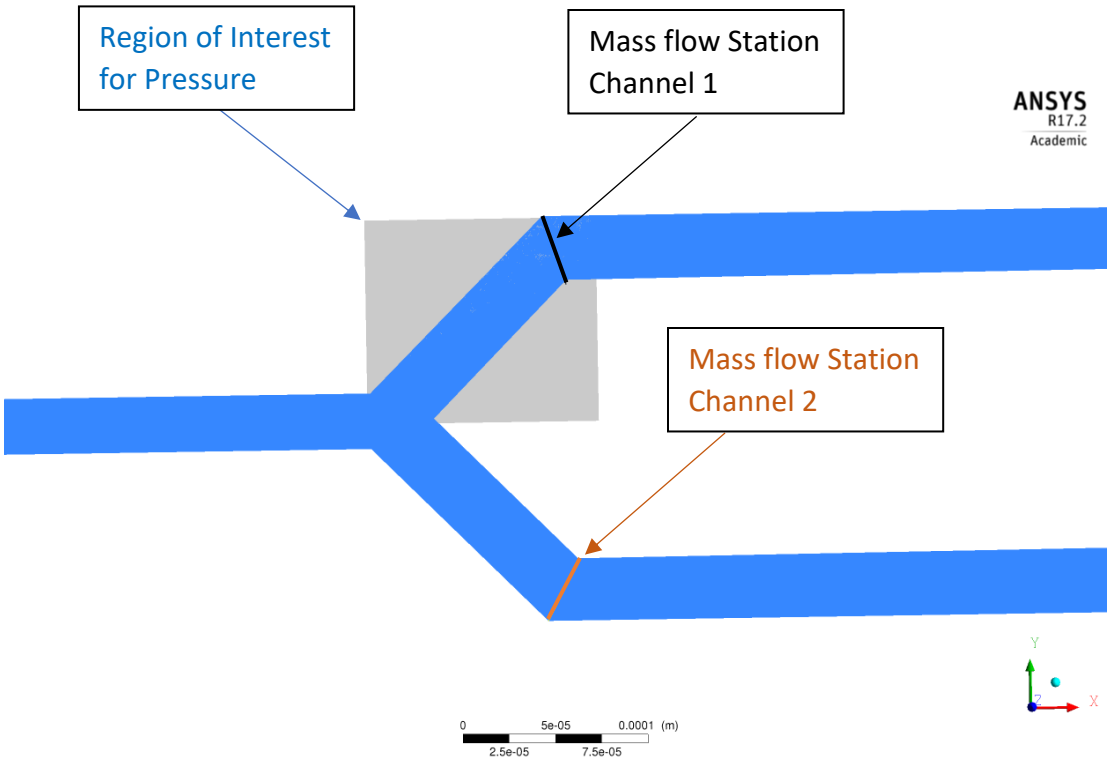

Figure 18, Regions of Interest Used to Calculate Metrics.

The grey region in the upper channel was sampled for pressure which was averaged. Mass flow across the black line in the upper channel defines $\dot{m}_{Channel\ 1}$; Mass flow across the Orange line in the lower channel defines $\dot{m}_{Channel\ 2}$.

To define the fluid's ability to return to steady state, a "sortability" metric was developed. Sortability compares the normal operating mass flow metric at steady state to the most settled mass flow metric at a given frequency. At low frequencies, the sortability will remain at one, indicating the streamlines can fully return to the steady state value. As the sorter frequency increases, the fluid starts being perturbed before it can fully return to the stable steady state solution. Sortability is defined by subtracting the mass flow metric of the desired frequency at the point nearest to steady state X_f from the steady state mass flow metric X_{ss}. To mimic the shape of a Bode plot for comparison, the difference of mass flow metrics is subtracted from one which normalizes the metric from 1 being operating as intended to 0 being complete reversal at time of sort.

$$S = 1 - (X_f - X_{ss})$$ *Equation 11*

4 Results

4.1 Three Dimensional Multiphase Results

4.1.1 Comparing Computational Results with Experimental results

The steady state solutions to three flow rate ratios are shown with their experimental counterpart in Figure 19.

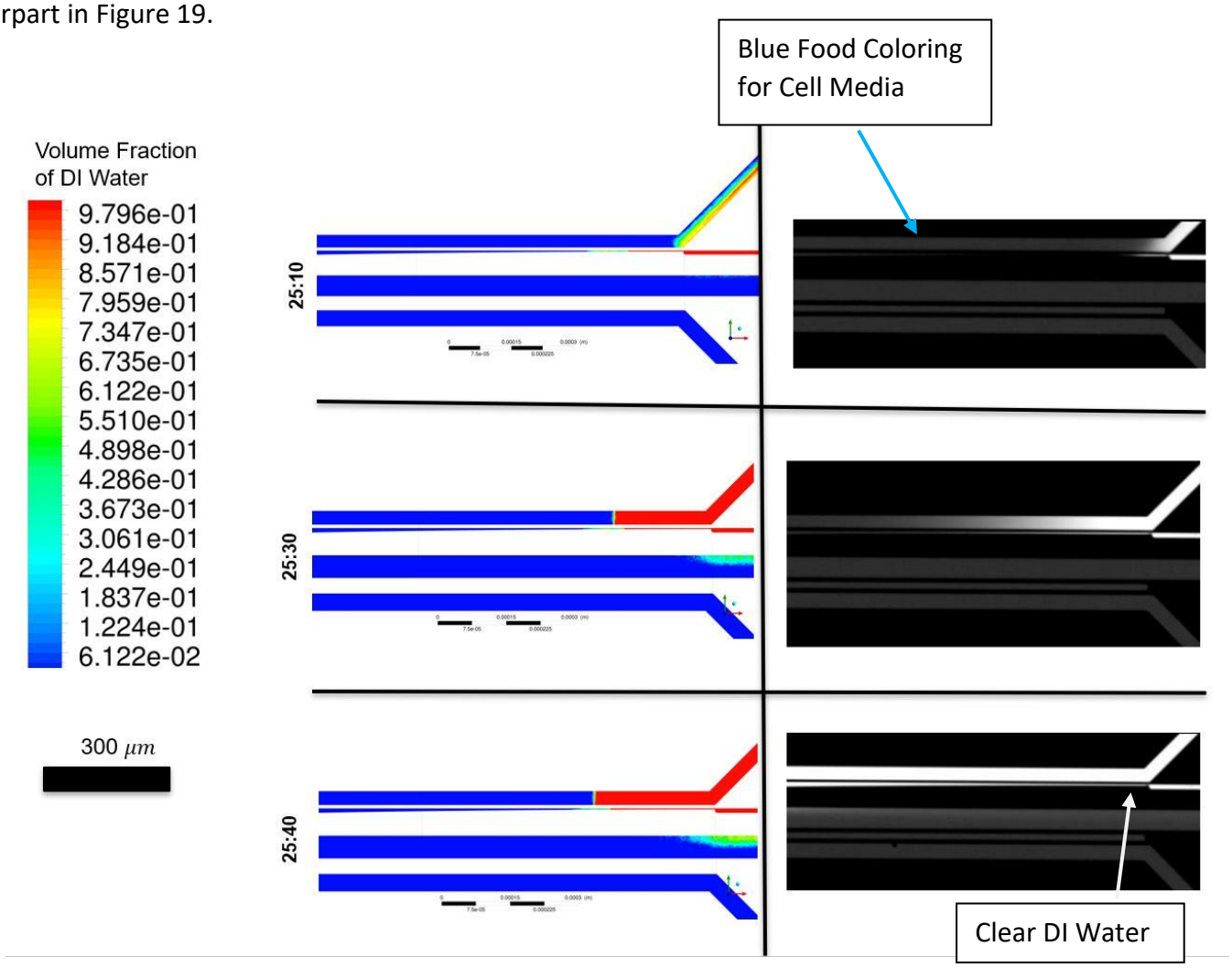

Figure 19, Comparing calculated and experimental DI water Volume Fractions at different flow rates.

Scale bar corresponds to both experimental and computational results.

The experimental set-up used Blue dye for the Cell solution which shows up grey; the DI water was clear and shows up as white. The Computational results display red as DI water, and Blue as cell solution. For all flow rates tested and shown in Figure 19, the DI water spills over the actuator into channel 1. For the 25:30 and 25:40 $\frac{\mu L}{hr}$ tests, the DI water stagnates in channel 1 as it meets the cell solution.

4.1.2Initialization Sensitivity

To test initialization independence, two cases were developed. In case 1, the initial conditions used in the other multiphase calculations was defined. Case 2 was set up to closely match the second distribution seen in experimentation (Figure 10). The initial distribution and steady solutions of tests relating to initialization independence are shown in Figure 20.

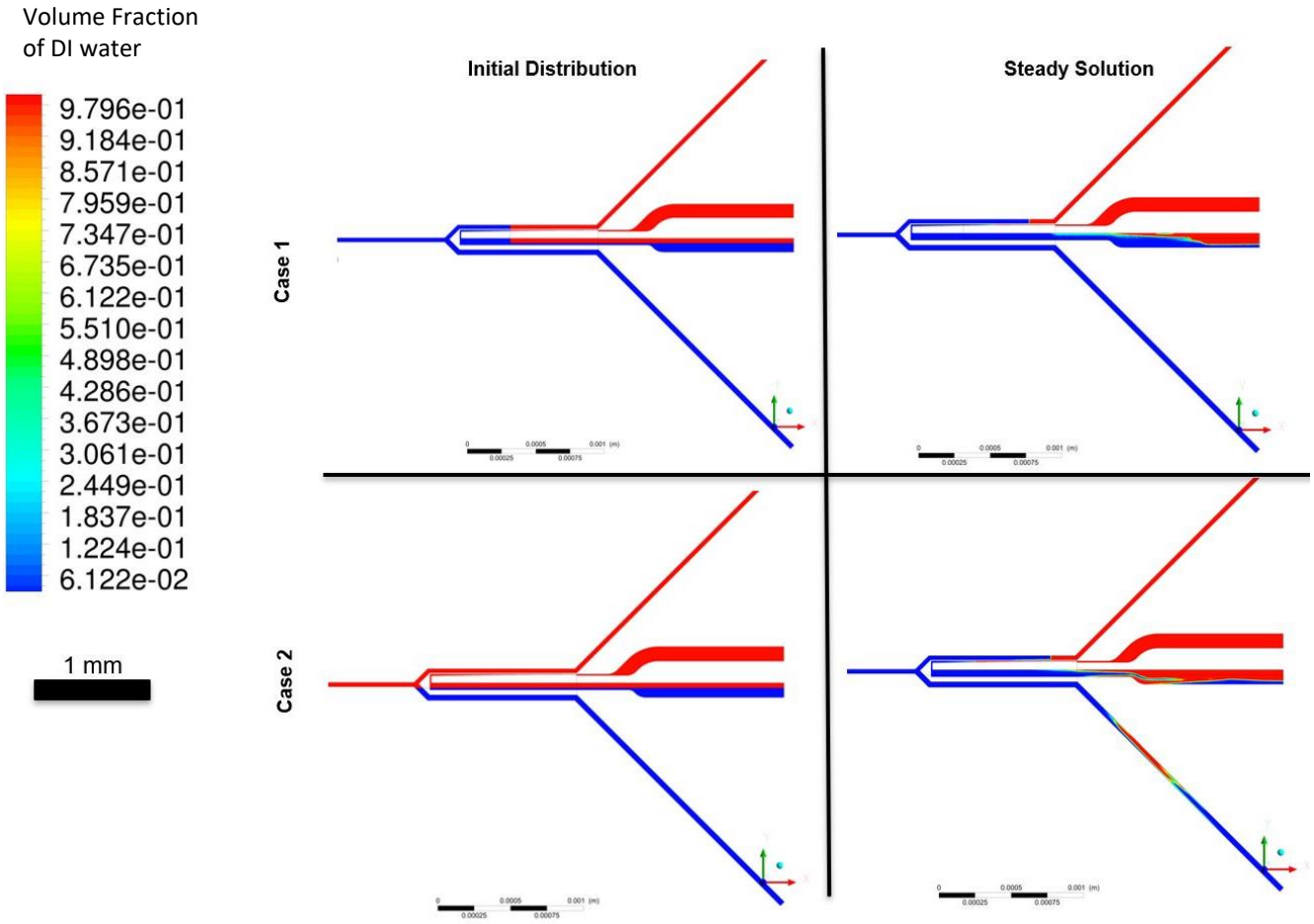

Figure 20, Comparing Steady State Results for Different Initial Distributions of DI Water.

The Distributions were chosen based on steady state behavior found in experimentation.

4.2 Two-Dimensional Transient Sorting

4.2.1 Pressure Contour at Different Times for 100 hz

The pressure contours and the streamlines traced from inlets and outlets are shown with indicators of what stage of sorting the image is from in Figure 21.

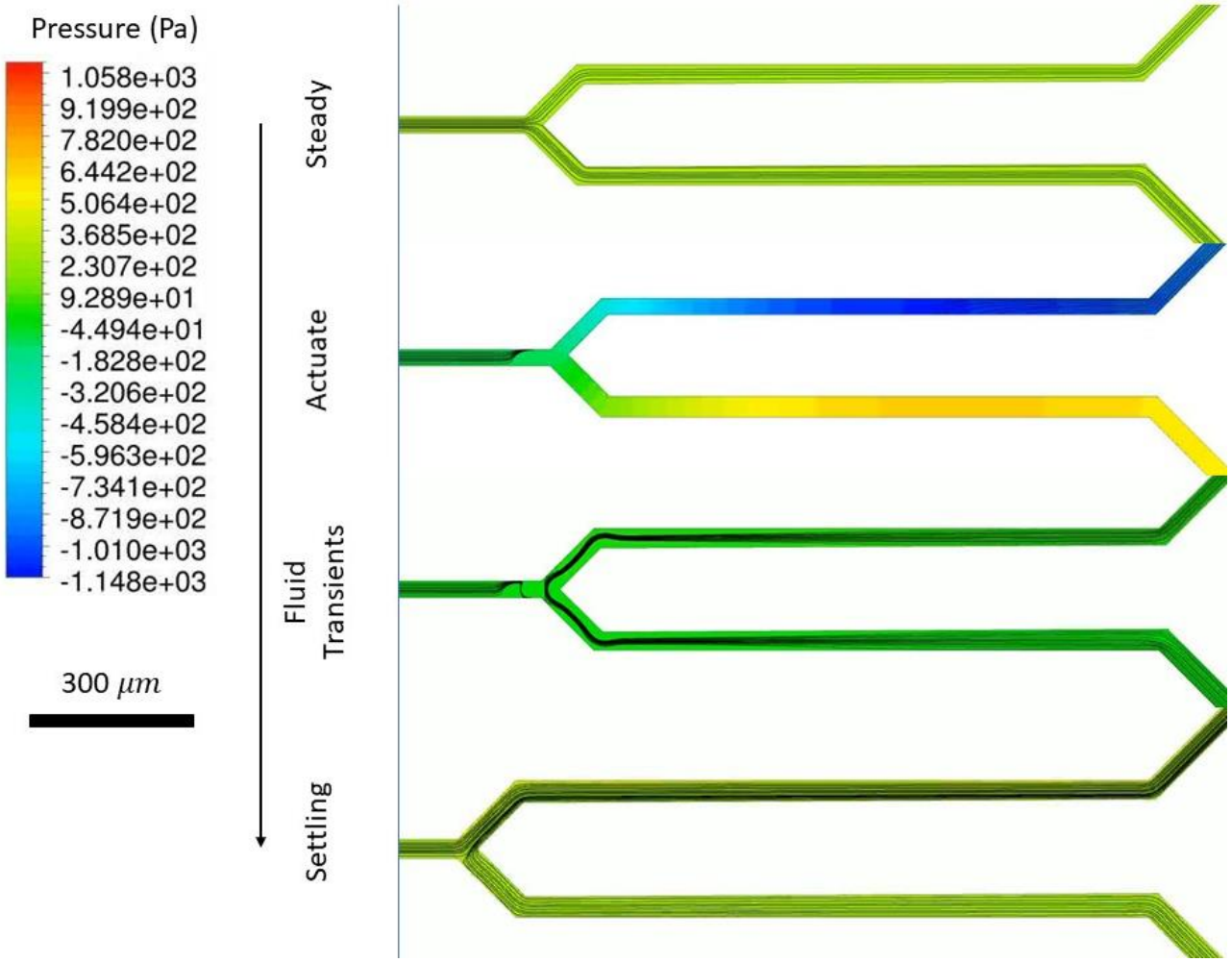

Figure 21, Pressure Contour and Streamlines of Two Dimensional Sorter during Sorting.

The motion of the sorter moves from steady through Transient before returning to steady. In steady state, the fluid streamlines have settled and will remain that way until a sorting event occurs. During the actuation, the actuator rotates downwards causing large pressure gradients in the sorter. During fluid transients, the fluid responds to the large pressure gradients from the Actuation with reversed flow. As the flow settles, the reversed flow slows until the inlet once again dominates the flow field.

4.2.2 Metrics vs. Time at 100 hz

To quantitatively analyze the operation of the sorter, the mass flow metric and pressure at their regions of interest were calculated over all recorded timesteps.

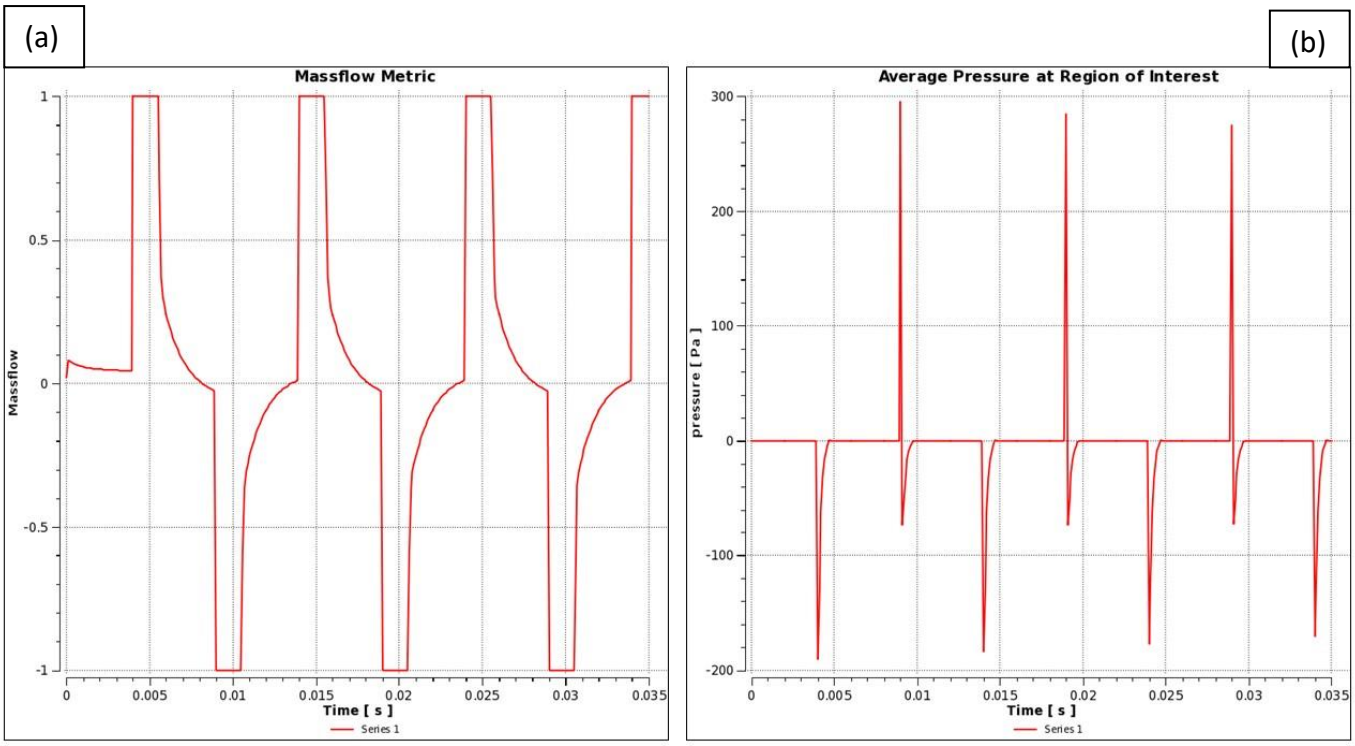

Figure 22, Raw Metrics at 100 hz plotted vs. Time.

In Figure 22a, the Mass flow metric vs. time calculated from Equation 10. The average pressure in the region of interest vs. time is plotted in Figure 22b. Both plots include the initial convergence before the sorter actuates and operate at 100 hz. A positive average pressure would mean the sorting is biased towards channel 2 which corresponds to the “OFF” state; A negative average pressure would mean the sorting would be biased to channel 1 which corresponds to the “ON” state. A positive mass flow metric means the flow is biased through

channel 1 which corresponds to the “ON” State, and vice versa is true for a negative. At 1 or -1, all the flow is going through one channel and out the other meaning total flow reversal and a stagnation before the bifurcation. At 0, the flow is evenly split between both channels.

4.2.3 Comparison of Metrics at Multiple Frequencies

The large pressure spikes present in the sorter and the need to compare different frequencies at once requires a different treatment. To compare several frequencies, the metrics are plotted against a normalized time which ranges from the start a sort at 0 to the end of a sort at 1. To accommodate the large pressure spikes, the pressure plot is cropped by a factor of 10^6 to better view the steady state behavior of the pressure metric.

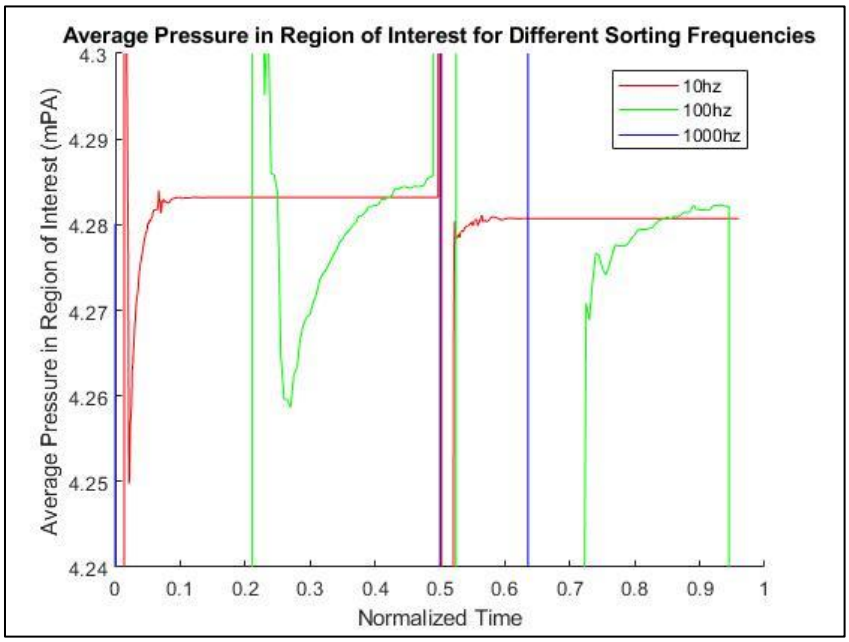

Figure 23, Average Pressure in the Region of Interest at All Tested Frequencies.

The Average Pressure in the Region of Interest metrics at all the tested frequencies plotted versus the normalized time which consists of a full sort cycle

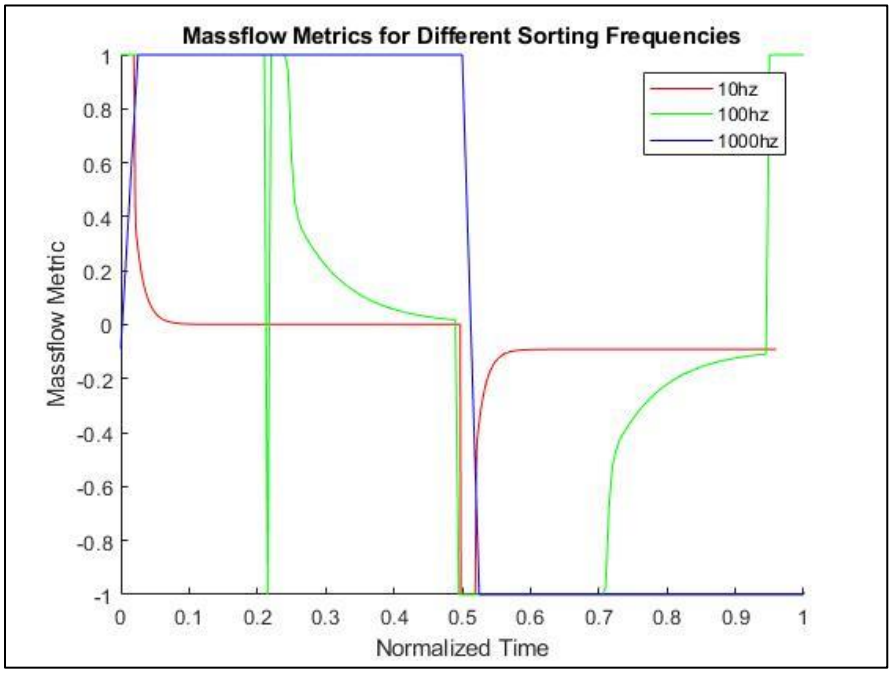

Figure 24, Mass Flow Metric at All Tested Frequencies.

The Mass Flow metrics at all the tested frequencies plotted versus the normalized time which consists of a full sort cycle

4.2.4 Determining Sortability at Different Frequencies

Sortability is plotted vs. frequency on a log scale along with the Bode plot of the actuator dynamics developed from the UDF in Figure 25.

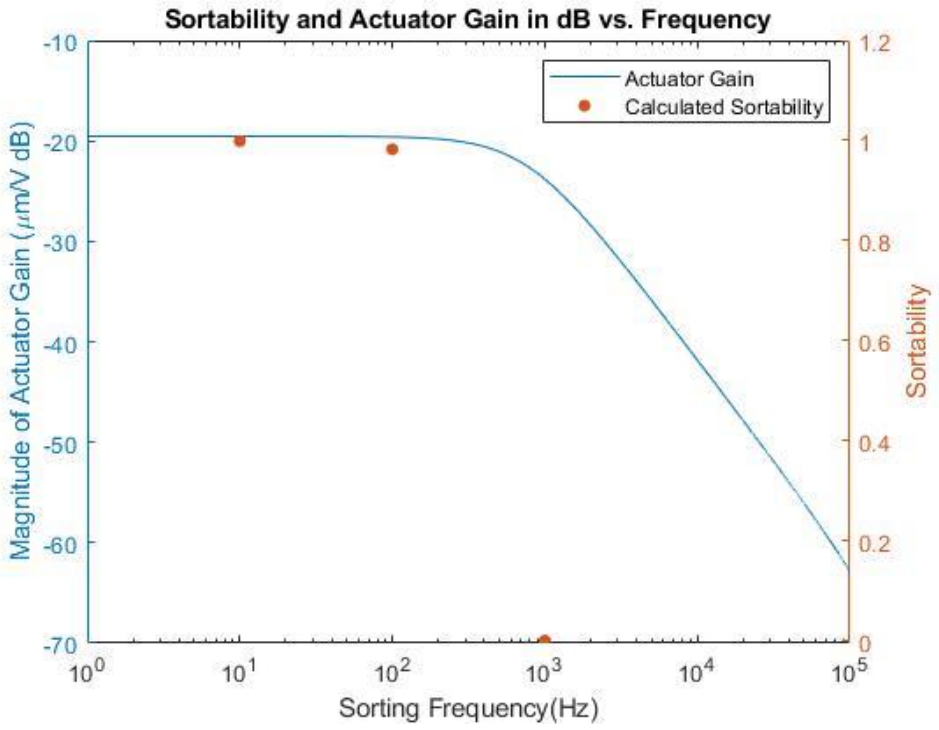

Figure 25, Sortability and Actuator Gain in dB vs. Frequency

The sortability is plotted along the right y-axis in yellow. The calculated values are represented by dots. The Bode Plot of the sorter calculated from the UDF is plotted along the left y-axis in blue.

5 Discussion

5.1 Multiphase Analysis

In Figure 19, the multiphase flow exhibits behavior that not only reduces viability of cells in the sorter, but also prevents the actuator from activating. This is because of the lack of DI water in the DI water channel in all the tested cases. For the 25:30 and 25:40 $\frac{\mu L}{hr}$ cases, a stagnation point is formed in channel 1 which prevents cells from moving down channel 1. One potential option to help mitigate DI water spillage would be to decrease the height of the recess above and below the actuator. Decreasing the gap would increase the hydrodynamic resistance above and below the actuator forcing more fluid into the DI water channel.

To test initialization independence, two distributions were chosen based on experimental work conducted by Melinda Lake shown in Figure 10. Both distributions converge to the same steady state solution in CFD in Figure 20. It is believed that one reason this occurs is because of limitations in the multiphase model chosen for this thesis. Because stagnation points are occurring in the sorter, the miscibility of the fluid becomes the primary transportation method for the two phases. This shortcoming can be seen when comparing the gradients of the fluids at the stagnation point for CFD and Experimental results. For the CFD results, the gradient is highly discontinuous, where as in the experimental results the gradient is smooth. The difference in gradients shows that the fluid is mixing in a way not captured by CFD in its current set up. Since the VOF model doesn't calculate mixing effects, a more complex model such as the Eularian model would be required to more closely match the experimental results [22].

5.2 Transient Analysis

During the operation of the sorter, large spikes in massflow metric and pressure are seen directly as the sort occurs in Figure 22. The pressure plot's transients die down faster on a whole than the mass flow metric's plot implying the inertial timescale is larger than the pressure timescale. Based on the plot of sortability in Figure 25, the maximum sorter frequency is between 100 and 1000 hz. Because the simulation was converted to two dimensions, the solution represents the "worst case scenario" for the sorter design. In 2 dimensions, the calculated pressure gradients are higher because there are fewer directions for the flow to move to accommodate that pressure gradient. In the three-dimensional case, flow could spill over and below the actuator at the tip to relive the pressure gradients. In terms of sorting, the

new path for the flow could cause issues if cells are forced above or below the actuator by the pressure gradients.

6 Conclusion

The purpose of this project was to analyze and provide engineering insight into a microfluidic cell sorter design. The analysis was split into two problems: how the multiple fluids present in the sorter interacted with each other, and how the actuator's motion effected the maximum sorting rate. It was determined from multiphase analysis that the current design of the sorter prohibited operation due to spillage of DI water into Cell Channel 1. Reducing the gap size between the actuator and the substrate as well as the gap between the actuator and the PDMS cap could stabilize the flow in the DI channel. The transient analysis performed showed that for the two-dimensional model of the sorter, the maximum sorting rate is between 100 and 1000 hz. At 100hz, there is a slight drop off in the sortability metric, however the degree of drop off can't be seen without running more test cases.

6.1 Future Work

A mesh refinement study conducted to ensure the validity of the results should be completed to ensure the results are mesh independent. To improve the accuracy of the multiphase metric, a different multiphase model should be utilized to account for the miscibility of the fluids in the sorter at potential stagnation points. To determine a more specific maximum sorting rate, more frequencies should be tested between 100 and 1000 hz. The two-dimensional model indicates a "worst case scenario" of the sorter, and the actual maximum sorting rate of the three-dimensional sorter could be higher due to three dimensional effects. To improve the accuracy of the sortability metric, three-dimensional analysis should be

conducted on the sorter. Particle tracking could be utilized in ANSYS Fluent to test and ensure the sortability metric accurately predicts the sorters behavior. Finally, combining the multiphase modeling with the transient analysis would provide a comprehensive model and answer the question of how the actuator's motion effects the DI water.

References

[1] L. J. Wysocki and V. L. Sato, "'Panning' for lymphocytes: a method for cell selection," *Proc. Natl. Acad. Sci. U. S. A.*, vol. 75, no. 6, pp. 2844–2848, Jun. 1978.

[2] D. Mattanovich and N. Borth, "Applications of cell sorting in biotechnology," *Microb. Cell Factories*, vol. 5, p. 12, Mar. 2006.

[3] J. W. Semple, D. Allen, W. Chang, P. Castaldi, and J. Freedman, "Rapid separation of CD4+ and CD19+ lymphocyte populations from human peripheral blood by a magnetic activated cell sorter (MACS)," *Cytometry*, vol. 14, no. 8, pp. 955–960, Nov. 1993.

[4] I. C. Clift, "Diagnostic Flow Cytometry and the AIDS Pandemic," *Lab. Med.*, vol. 46, no. 3, pp. e59–e64, Aug. 2015.

[5] "(PDF) The Application of Flow Cytometry in the Clinical Setting of HIV," *ResearchGate*. [Online]. Available: https://www.researchgate.net/publication/303692390_The_Application_of_Flow_Cytometry_in_the_Clinical_Setting_of_HIV. [Accessed: 31-Mar-2019].

[6] J. J. Agresti *et al.*, "Ultrahigh-throughput screening in drop-based microfluidics for directed evolution," *Proc. Natl. Acad. Sci.*, vol. 107, no. 9, pp. 4004–4009, Mar. 2010.

[7] "Flow Cytometry (FCM) /FACS | Fluorescence-activated cell sorting (FACS)." [Online]. Available: https://www.sinobiological.com/flow-cytometry-fcm-facs-fluorescence-activated-cell-sorting-facs.html. [Accessed: 11-Apr-2019].

[8] T. Franke, L. Schmid, D. A. Weitz, and A. Wixforth, "Magneto-mechanical mixing and manipulation of picoliter volumes in vesicles," *Lab. Chip*, vol. 9, no. 19, pp. 2831–2835, Oct. 2009.

[9] J. Zhao and Z. You, "Spark-generated microbubble cell sorter for microfluidic flow cytometry," *Cytometry A*, vol. 93, no. 2, pp. 222–231, 2018.

[10] T. Franke, A. R. Abate, D. A. Weitz, and A. Wixforth, "Surface acoustic wave (SAW) directed droplet flow in microfluidics for PDMS devices," *Lab. Chip*, vol. 9, no. 18, pp. 2625–2627, Sep. 2009.

[11] "Sort-synchronization control in microfluidic loop devices with experimental uncertainties using a model predictive control (MPC) framework - ScienceDirect." [Online]. Available: https://www.sciencedirect.com/science/article/pii/S1474667016443806?fbclid=IwAR0EtZVEGTVRMU8IdtmqtSBdBIUSDTS3l5_v2EE1nJJFem6NJb53RAMmnhM#bbib13321. [Accessed: 12-Apr-2019].

[12] M. M. Wang *et al.*, "Microfluidic sorting of mammalian cells by optical force switching," *Nat. Biotechnol.*, vol. 23, no. 1, pp. 83–87, Jan. 2005.

[13] R. D. Lewis, J. W. Foreman, H. J. Watson, and J. R. Thornton, "Laser Doppler Velocimeter for Measuring Flow-Velocity Fluctuations," *Phys. Fluids*, vol. 11, no. 2, pp. 433–435, Feb. 1968.

[14] H. A. Stone, *Introduction to Fluid Dynamics for Microfluidic Flows*. .

[15] B. S. Preetham, M. A. Lake, and D. J. Hoelzle, "A curved electrode electrostatic actuator designed for large displacement and force in an underwater environment," *J. Micromechanics Microengineering*, vol. 27, no. 9, p. 095009, Aug. 2017.

[16] V. Mukundan and B. L. Pruitt, "MEMS Electrostatic Actuation in Conducting Biological Media," *J. Microelectromechanical Syst. Jt. IEEE ASME Publ. Microstruct. Microactuators Microsens. Microsyst.*, vol. 18, no. 2, pp. 405–413, Apr. 2009.

[17] “FLUENT 6.3 User’s Guide - 25.22.1 Judging Convergence.” [Online]. Available: https://www.sharcnet.ca/Software/Fluent6/html/ug/node1067.htm. [Accessed: 27-Mar-2019].
[18] “5.2.2. Mesh Quality.” [Online]. Available: https://www.sharcnet.ca/Software/Ansys/17.0/en-us/help/flu_ug/flu_ug_mesh_quality.html. [Accessed: 27-Mar-2019].
[19] “FLUENT 6.3 User’s Guide - 23.3.1 Overview and Limitations of the VOF Model.” [Online]. Available: https://www.sharcnet.ca/Software/Fluent6/html/ug/node881.htm. [Accessed: 27-Mar-2019].
[20] “10.6.2. Dynamic Mesh Update Methods.” [Online]. Available: https://www.sharcnet.ca/Software/Ansys/16.2.3/en-us/help/flu_ug/flu_ug_dynam_mesh_update.html. [Accessed: 27-Mar-2019].
[21] John Anderson, *Fundamentals of Aerodynamics*, 6th ed. McGraw-Hill Ediucation.
[22] “FLUENT 6.3 User’s Guide - 23.5.1 Overview and Limitations of the Eulerian Model.” [Online]. Available: https://www.sharcnet.ca/Software/Fluent6/html/ug/node901.htm. [Accessed: 27-Mar-2019].

Appendix

C code used for 1000 hz before being compiled into Fluent:

```
#include "udf.h"
#include "math.h"


DEFINE_CG_MOTION(object_mov, dt, vel, omega, time, dtime)


{


/*Global Constants*/


real f, pi, r, m, b, k, A, T, itter, w, mag, phase, omega_temp, j,
delay,threshold;


f = 1000; /*frequency of input*/
pi = 3.14159;
r = 0.00234; /*Radius of Rotation in Meters*/


/*transfer function constants*/
```

```
m = 1.6455e-9 ; /*mass of system*/
b = 1.96233e-3;
k = 9.47;

/*Fourier Series constants*/
A = 10; /*volts*/
T = pow(f,-1);

itter = 1000;
omega_temp = 0;
delay = 0.004;
threshold = 60;

if (time <= delay) {
omega_temp = 0;
}

else {

for (j = 1 ; j <= itter ; j++)
  /*Calculate Phase*/
  { w = 2*pi*j*(1/T);
    mag = pow(pow(-m*pow(w,2) + k , 2)+pow(b*w,2) , -0.5);
    phase = -atan2( b*w , (-m*pow(w,2)) + k );

    /*Calculate Terms in Fourier Series*/
    omega_temp = omega_temp + mag*(A/(pi*j))*(1-
cos(pi*j))*cos(2*pi*j*(1/T)*(time-delay) + phase)*2*pi*j*(1/T);

}

omega_temp = (omega_temp + A/(2*k))*pow(10,-4)/(r*1.0241*5.4);
}
```

```
/* Reduce Noise Caused by Fourier Series*/
if (omega_temp < threshold && omega_temp > -threshold){
omega_temp = 0;
}

omega[2] = omega_temp; /*Correct for direction*/
omega[1] = 0;
omega[0] = 0;

Message ("Omega Is %g \n", omega[2]);

vel[2] = 0;
vel[1] = 0;
vel[0] = 0;

}
```